Controlled Chemical-Patterning of Textile to Accelerate Anti-gravity Water Flow

*Saurav Kumar,[a] Angana Borbora,[a] Pritha Chakraborty,[a] Hrisikesh Sarma,[a] Ashutosh Bandyopadhyay,[d] Akash Bose,[a] Biman B. Mandal,[b,c,d] Mizuki Tenjimbayashi,[*e] Uttam Manna[*a,b,c]*

Affiliations

[*][a] Department of Chemistry, Indian Institute of Technology Guwahati, Assam, 781039 India
E-mail: umanna@iitg.ac.in
[b] Centre for Nanotechnology, Indian Institute of Technology Guwahati, Assam 781039 India
[c] Jyoti and Bhupat Mehta School of Health Science & Technology, Indian Institute of Technology Guwahati, Assam, 781039 India,
[d] Biomaterials and Tissue Engineering Laboratory, Department of Biosciences and Bioengineering, Indian Institute of Technology Guwahati, Guwahati, Assam, 781039 India
[*][e] Research Center for Materials Nanoarchitectonics (MANA), National Institute for Materials Science (NIMS), Tsukuba, Ibaraki, Japan
E-mail: TENJIMBAYASHI.Mizuki@nims.go.jp

Keywords: Patterned textile • Moisture managment • superhydrophobicity • Anti-gravity transport • 1,4-conjugate addition reaction

Abstract

Bio-inspired unidirectional flow of tiny aqueous droplets across the fibrous substrate paved the way for the emergence of various advanced materials related to body moisture management, thermal management, accelerated wound healing, water harvesting, etc. In the past, textiles decorated with non-contact based wettability-patterns enabled unidirectional water flow—without flooding the top surface by the transferred water. However, such approaches mostly suffered from a low (~ 0.176 µL mm^{-2} s^{-1}) flow rate, and likely to delay the overall liquid ejection process. Here, we introduced a chemically reactive coating capable of tailoring water wettability (121.3°± 2.4° to 153.3°± 1.8°) on commercially available textiles to develop chemically modulated wettability-pattern for achieving a rapid (2.57 ± 0.28 µL mm^{-2} s^{-1}) flow rate of water against the gravity with an ability of rolling the accumulated liquids on the top surface. The spatially selected and controlled chemical modification with hydrophilic and hydrophobic small molecules through a 1, 4-conjugate addition reaction yielded a three-dimensional channel with a customized wettability gradient. The pinning and depinning of invaded water through such chemically decorated channels enabled unidirectional and fast penetration of liquid, where the water penetration resistance largely depends on the water penetration direction and dimension of the chemically modulated channels.

Introduction

In nature, many living objects adopted different strategies for the unidirectional liquid flow for their survival. For example, asymmetric spines in cactus,[1, 2] periodic spindle knots in spider silk,[3, 4] bird beaks,[5, 6] and peristome surface structure of pitcher plants [7-10] inherently display a unidirectional flow of water. Inspired by these naturally existing interfaces, various macroscopic and microscopic asymmetric structures of naturally existing interfaces were mimicked artificially to achieve unidirectional liquid transportation—which finds diverse potential applications—including water harvesting,[2, 11] oil/water separation,[12,13] heterogeneous catalysis,[14, 15] smart textile,[16, 17] etc. In contrast to asymmetric bio-inspired structures, Whitesides and coworkers introduced a gradient of wettability to achieve another type of unidirectional water transport, where water droplets run 'up the hill' without requiring any external energy.[18] Since then, few other approaches—including water column-assisted coalesce of tiny water droplets across superhydrophobic barrier,[19] patterned channel with wettability gradient,[16, 17, 20-23] and Janus wettability across a fibrous substrate[24-29] were introduced for liquid transport against gravity. Among these, the approach of patterned channels with liquid repellent background not only provides a facile basis for the anti-gravity transport of water but also prevents the flooding of the top surface by the transferred liquid. Moreover, such a design allows the rolling of transferred water droplets to keep the top interface dry.

Transportation of secreted body waste found in the form of tiny aqueous droplets on the skin (widely recognized as sweat) is of great challenge as the flooding of commonly used hydrophilic textiles by the secreted aqueous body waste (i.e. sweat) led to a prolonged exposure to an unhealthy and uncomfortable environment.[30] An average person is known to produce sweat with a rate of ~ 1 $Kgm^{-2}h^{-1}$[31] under a condition of moderate exercise, whereas the water repellent commercially available fabrics remained capable of rejecting sweat at a much lower rate, i.e., ~ 0.46 $Kgm^{-2}h^{-1}$.[32, 33] To achieve better management of personal moisture, recently, the principle of anti-gravity transport of liquid is successfully applied in designing a 'skin-like' fabric to eject sweat from body surface to keep the body skin dry and relatively cool—with respect to its surroundings.[21] In a seminal report, a superhydrophobic background derived from perfluorosilane-coated TiO_2 nanoparticles was subjected to spatially selective plasma treatment to develop gradient wettability spot channels for unidirectional water transport.[16] Thereafter, various other patterned channels were introduced by strategic modulation of pore and wettability of used fibrous substrates.[17, 20, 22, 23] However, the use of environmentally toxic fluorinated chemistry in the superhydrophobic backgrounds and the low flow rate of water transfer (< 0.2 μLs^{-1}) demand further design of material for rapid ejection of relevant liquids

(e.g., bio-fluids, sweat and so on) across the selected fibrous substrate for its more realistic and prospective applications in the efficient management of personal moisture, wound healing, design of liquid diode etc.

Various natural or synthetic fabrics have complex geometries and tend to rapidly absorb water and other liquids, leading to arbitrary spillage. This has made contact-based controlled chemical patterning on fabric challenging in the past. In the previous literature, mostly, non-contact patterning methods (UV-ray, plasma treatment, etc.) were spatially selectively applied to perturb the hydrophobic chemical groups (e.g., fluorinated hydrocarbons) on hydrophobic/superhydrophobic interface (Table S1); however, controlled and uniform penetration of UV-radiation or plasma across the highly opaque fibrous substrate would be a challenging task to achieve. On the other side, to restrict the arbitrary absorption of water or other solvents during spatially selective chemical modification, a liquid repellent and chemically reactive coating on fabric is essential. To the best of our knowledge, examples of chemically reactive superhydrophobic coating on fabric are rare in the literature. While the residual reactivity allowed a controlled chemical modification, the embedded water repellence restricts arbitrary spillage of modifying solution during the course of wet chemistry on fabric, ensuring a controlled and spatially selective pattern wettability across its thickness as depicted in Scheme 1. As the current method is substrate independent, we can successfully develop a wettability patterns on a wide range of natural and synthetic fabrics (Table S1) at ambient conditions—without requiring any instrument.

Here, a chemically reactive nanocomplex (CRNC) was dip-coated on the selected fibrous substrate for direct and spatially selective modulation of wettability through adopting a 1, 4-conjugate addition reaction in aqueous medium at ambient condition, referred as ‘wet-chemistry’ using selected small molecules—i.e., glucamine as depicted in Scheme 1A-D. In the current approach, no sophisticated instrumental set-up is required—rather, the diameter and depth of the patterned spot can be regulated easily—just by controlling the contact area between the textile and aqueous droplet of glucamine and the duration of wet chemistry. The hydrophilic moiety is installed—without perturbing the hydrophobic moiety (e.g., hydrocarbon) to spatially selectively modulate the water wettability on the water-repellent interface (Scheme 1E). The prepared patterns provided superior anti-gravity transport of water irrespective of the channel diameters (D) that were commonly adopted in the reported literature on patterned textiles, as shown in Scheme 1F. This is likely due to the chemically controlled optimization of pattern dimension with gradient of wettability on a water repellent background (Scheme 1E). In the current strategy, chemically modified hydrophobic and hydrophilic moiety present in the

patterned channel contribute to a unidirectional pinning and depinning process to transport the beaded water droplet against the gravity, where both water friction force of transported water and breakthrough pressure varies depending on the channel size and hydrophobicity of background of the prepared channel. Such material remained successful in the rapid ejection of accumulated sweat from the skin to provide a dry and non-sticky environment. Moreover, the fast anti-gravity transport of artificial sweat ensures depletion of temperature by 4.2°C at a relevant and hot (40°C) outdoor condition, where the improvement in the performance of controlling body tempeteratute is found to be 40 % in comparison to the best available performance of patterned textiles in literature (Table S2). In addition, such a strategy would be useful in intravenous therapy where unidirectional transport of saline and medicine would be possible—with an ability to prevent blood backflow.

Results and Discussions

Orthogonally reactive superhydrophobic textile

In the recent past, branched polyethylenimine (BPEI) and dipentaerythritol pentaacrylate (5Acl) were mutually reacted through 1, 4-conjugate addition reaction to prepare chemically reactive nanocomplex (CRNC) and its porous coatings on planar substrates provided a facile basis to independently tailor liquid (oil/water) wettability and adhesion property for anti-counterfeiting and naked eye chemical sensing applications.[34, 35] Inspired by these results, here, CRNC is deposited on an inherently hydrophilic and stretchable fibrous substrate (polyurethane (PU) fabric) to prepare orthogonally reactive polymeric coating (Figure 1A-F) for demonstrating anti-gravity flow of water without flooding the top surface of textile through introducing chemically-modulated patterned channels on a bio-inspired extremely water repellent background. The existence of residual chemical reactivities (i.e., amine and acrylate) was characterized with X-ray photoelectron spectroscopy (XPS) and Fourier-transform infrared spectroscopy (FTIR) analysis (Figure 1G, H). The deconvoluted XPS signatures at binding energy of 399.8 eV revealed the residual primary amine group—which diminished after mutual reaction with octadecyl acrylate (ODAc) through 1, 4-conjugate addition reaction as shown in Figure 1G. Consequently, the ODAc-modified coating displayed a significant rise in water contact angle (WCA) from 0º to 153º as shown in Figure 1C-F. Notably, the association of superhydrophobicity through ODAc modification was achieved without affecting the residual acrylate groups in the prepared coating as evident from the existence of the characteristic XPS peak for vinyl moiety at 284.1 eV as shown in Figure 1G. Similarly, the characteristic IR signature for C-H deformation of β carbon of the vinyl group at 1408 cm^{-1} remained intact with respect to an internal reference, i.e., IR peak for carbonyl stretching at 1712 cm^{-1} (Figure 1H).

Further, the orthogonal reactivity of available moieties (i.e., amine and acrylate)—towards mutual reaction with small molecules was separately validated with an optical fluorescence microscopic study as depicted in Figure S1.

In addition to superhydrophobicity, the modification of reactive coating with ODAc provided a relatively low (48.8 μN) force of water adhesion as shown in Figure 1I. Both water wettability and force of water adhesion of the prepared coating majorly depend on the length of hydrocarbon tails of selected alkyl acrylates (i.e. butyl acrylate (BAc), hexyl acrylate (HAc), octyl acrylate (OAc), lauryl acrylate (LAc) and ODAc) as shown in Figure 1I. Thereafter, the topography of the selected fibrous substrate (PU fabric) with and without polymeric coatings—and after their post covalent modifications with selected alkyl acrylates were characterized with field emission scanning electron microscope (FESEM; Figure 1J-M and Fig. S2). The smooth and featureless fibers (Fig. S2A, B) of PU fabric were decorated with globular domains due to the deposition of CRNC; however, no distinguishable change in globular domains was observed after modifying the reactive coating with selected alkyl acrylates (Figure 1J-M). Hence, the post chemical modification does not change the topology of the fabrics and the alkyl chain length in the selected modifiers remained the experimental variable to modulate water wettability in this current design.

Such coated textiles with tailored hydrophobicity remained chemically reactive because of the existence of a residual acrylate group. To independently validate the existence of chemical reactivity of the prepared superhydrophobic textile, a portion of it was subjected to modify with selected hydrophilic-small molecules—i.e., glucamine—which resulted in alteration of WCA from 153° to 0° (Figure 1N). The depletion of characteristic IR signature of vinylic C-H deformation at 1408 cm^{-1} (Fig. 1H) with respect to another invariable IR signature, i.e., carbonyl stretching at 1712 cm^{-1} supported the 1,4-conjugate addition reaction between amine of glucamine and residual acrylate of superhydrophobic coating. Further, the XPS study independently revealed the disappearance of characteristic peak for vinyl moiety at 284.1 eV as shown in Figure S3. Thus, an amine reactive superhydrophobic coating is successfully developed on the selected fibrous substrate.

1. Wet-chemistry based patterned textile.

In this section, the chemically reactive superhydrophobic coating applied on fibrous substrate was subjected to chemical modification with selected hydrophilic molecules in wet condition to prepare a Janus membrane, where one face of the coated fabric was selectively exposed to aqueous (concentration of 0.275M) solution of glucamine for different durations. The surface

of the prepared superhydrophobic textile that was directly exposed to an aqueous solution of glucamine is denoted as the top side, and the other surface of the textile is referred to as the back side. The gradual ingression of glucamine solution allowed to modify the chemically reactive superhydrophobic coating on the textile through 1, 4-conjugate addition reaction—which resulted in the depletion of WCA, as shown in Figure 2A. However, the trends for the apparent change in WCA of beaded water droplets on two different surfaces—i.e., the top and back sides of the same fabric- were distinct. Till 45 minutes of glucamine-treatment, the WCA on the top side was gradually depleted from 153° to 110°—whereas the back side remained extremely water repellent with static WCA of > 150°. After the exposure of glucamine-solution for 60 minutes, the top surface became hydrophilic with WCA ~ 41° and remained wet. However, the back side of the same fabric immediately soaked a beaded water droplet with an apparent WCA of 0° without leaving any trace of it on the back side. Eventually, this process yielded a Janus textile, where flooding of liquid was only observed on the top side—and back side remained dry as shown in Figure 2B. Thereafter, the penetration of the beaded aqueous phase across the coated—and chemically-modified textile was examined, where the mutual reaction duration between the selected modifier (i.e., glucamine) and the reactive superhydrophobic interface was gradually increased to 90 minutes. In this context, an aqueous solution of calcium salt was beaded on the modified textile to trace its spreading and soaking into the chemically modified coated textile, where alteration of water wettability from superhydrophobicity to hydrophilicity because of glucamine modification enabled the immediate infiltration of the aqueous phase in the modified textile. This process allowed the wetting of hydrophilic portion by beaded aqueous solution of calcium. Thus, the EDX mapping of selected metal ions in the textile provided a basis to track the penetration of aqueous solution of calcium ions in the modified textile, and so the thickness of chemical modification accross the superhydrophobic textile with glucamine (Figure S4). It is worth to mention that the glucamine present in its aqueous solution gets exposed to the reactive superhydrophobic textile to react with residual acrylate groups at the contact area between the reactive textile and bedaed aqueouse solution of glucamine. The contact area becomes partially hydrophilic and aqueous solution of glucamine wet the area and gradually penetrates into the reactive textile. On further chemical reaction, the interior of the reactive fabric became selectively hydrophilic. Hence, the penetration of calcium ions in the bulk of the textile (thickness of 456 ± 8 μm) was improved from 36.5 ± 4.2 μm to 456 ± 8 μm with increasing the exposure time of reactive superhydrophobic textile to aqueous solution of glucamine as shown in Figure 2C, D. Following this process, two distinct Janus textiles were obtained, where the chemically reactive

superhydrophobic textile was individually exposed to aqueous solution of glucamine for 60 minutes and 75 minutes, where both of them displayed soaking of beaded water at back-side of Janus textiles (denoted as JT_{60} and $JT_{75,}$ respectively) with apparent WCA of 0° (Figure 2E, F)—but having differences in thickness of chemical modification—i.e. 291.8 ± 6.4 μm μm and 401.2 ± 6.8 μm (Figure 2E, F). These two Janus textiles are embedded with distinct abilities towards unidirectional and anti-gravity transfer of aqueous phase under identical experimental set-up. As expected, beaded droplets of water (200 μL) on the top side of both Janus textiles failed to filtrate into the back side under the gravity. However, tiny droplets of blue-coloured water (because of added methylene blue dye) readily passed through the membrane against gravity to reach out to the beaded droplet of water on the top side of both Janus textiles (Figure 2E and Movie 1). However, JT_{75} remained capable of unidirectional and anti-gravity transfer of only 460 μL of aqueous phase, beyond this volume, the transferred water flowed back to the back side of the textile (Figure 2F). In contrast, JT_{60} remained efficient in transferring a relatively large volume (1.5 mL) of water against gravity—without having any reverse flow to its bottom side (Figure 2E). The thickness of chemical modification in these Janus textiles is likely to contribute in such distinct ability towards unidirectional and anti-gravity transfer of aqueous droplets. The prepared JT_{60} remained efficient to display the anti-gravity transfer of water in absence of beaded water droplet on top, however, transferred water readily spread on the top side because of the embedded hydrophilicity as shown in Figure S5. Such phenomenon is common for other Janus textile as well. However, to restrict such arbitrary spreading and spilling of transferred water on top of the Janus textile, a patterned textile with Janus channels on superhydrophobic background is developed—following spatially selective chemical modification of chemically reactive superhydrophobic textile. In this current strategy, the beading of tiny droplets of aqueous solution of glucamine allowed mutual and spatially selective reaction with residual acrylate groups present in the chemically reactive superhydrophobic textile through 1,4-conjugate addition reaction at the contact of textile and aqueous droplet, where the embedded superhydrophobicity restricts the random spreading of aqueous solution of glucamine on the fabric. As a consequence, the beaded droplet of aqueous solution of glucamine was found to be slowly absorbed by the reactive superhydrophobic coating over time—without leading to any arbitrary spillage (Figure S6A). Further, the gradual change in the percentage of the height of the beaded droplet and the depletion of water contact angle (Figure S7A) suggested the 1,4-conjugate addition reaction between amine of glucamine and residual acrylate of reactive superhydrophobic textile at the place of contact between the beaded water droplet and reactive superhydrophobic coating. In the absence of glucamine molecules, the beaded

droplet of DI-water on the reactive superhydrophobic textile absolutely failed to display such a drastic change in water contact angle as shown in Figure S6B. Moreover, the diameter and depth of the chemically modulated patterned pattern on the superhydrophobic background gradually increased with time as shown in Figure S7B-C. Thus, the current approach provided a basis to tune the dimension of the patterned channel through a direct chemical modification at ambient conditions. Eventually, a pattern textile with Janus channel on superhydrophobic background was achieved following contact based selective 'wet-chemistry' as shown in Figure 2H. As expected, a distinct change in water wettability was observed on both pattering top-spot and pattering back-spot because of this chemical modification with times as shown in Figure S8. While, the channel is decorated with hydrophilic and hydrophobic moieties, the covalently attached octadecyl moiety contributed to the background superhydrophobicity as depicted in Figure 2H. Importantly, the volume of beaded aqueous droplet of glucamine controls the dimension of patterned channel on superhydrophobic background. Thus, the droplet contact area to the fabric controls the diameter of patterning, and the patterning time decides the depth of the pattern as illustrated in Figure 2G, which makes this process highly versatile. After that, the prepared patterned textile was partially inverted at its bottom right corner to display the beading behavior of the water droplets on its top and bottom surfaces. Water droplets beaded at the pattering top-spot (denoted with a black dotted circle in Figure 2I) with low WCA, while the patterned back-spot readily soaked the beaded blue-colored water droplets, as indicated by the white dotted circles in Figure 2I. As expected, the background of the patterned channel displayed extreme water repellence, as shown in Figure 2I. Thereafter, morphology of the patterned textile was examined. No significant change in topography was observed between the top and back sides of the textile—irrespective of patterning and background regions as shown in Figure 2J. Such change in wettability of beaded water droplet attributes to the spatially selective chemical-modification of reactive superhydrophobic textile with glucamine.

Thereafter, a droplet of water was placed on the patterned top-spot of a patterned textile prepared by exposing to glucamine solution spatially selectively for 60 and 75 minutes, denoted as PT_{60} and PT_{75}, respectively. On exposing a tiny droplet of dyed water (blue color) on the patterning back-spot, an immediate anti-gravity transfer of the water was noticed—without having any arbitrary spreading of transferred water on the top surface as illustrated in Figure 2K. However, distinct results towards anti-gravity water transfer were noticed for patterned textiles, i.e. PT_{60} and PT_{75}, after transferring the water droplets beyond a certain volume (70 μL). A 50 μL droplet of water was individually placed on the patterning top-spot of both PT_{60} and PT_{75}, where the water droplet beaded with different apparent contact angles due to distinct

infiltration of water into the patterned textiles as shown in Figure 2L and Movie 2. Initially, an instant anti-gravity transfer of water was observed for both patterned textiles—but the backflow of the transferred liquid to the bottom surface of PT_{75} (Figure 2L and Movie 2) was noticed just after transferring 70 μL of water through back-spot. However, PT_{60} remained successful in transferring water more than twice (i.e., at least 150 μL; Figure 2L) amount against gravity, without failure at an identical experimental condition. It is likely due to the decrease in the breakthrough pressure—that resists the backflow of transfer water under gravity. The alteration of breakthrough pressure on such a pattern interface is discussed later in detail. Thereafter, to examine the impact of the relative volumes of beaded and tiny droplets on anti-gravity water transport behavior through this patterned textile, volumes of water droplets exposed at the lower surface were gradually varied from 0.5 μL to 5 μL, keeping the beaded water droplet volume (i.e., 5 μL) constant on the top surface (Figure S9). The patterned fabric successfully transported water droplets against gravity, irrespective of the volume ratio of water placed on top and lower surfaces (Figure S9). In fact, without a beaded water droplet on the top surface, the water droplets were successfully transported against gravity, irrespective of their volume use, as shown in Figure S10. Thus, the prepared patterned textile works regardless of the volume of water droplets, and it continued to perform both in the presence and absence of beaded water droplets on the top of the patterned textile. Moreover, the continuous exposure of water droplets at the back-spot allowed to rapidly transport it against the gravity. It accumulated at the top-spot of the patterned textile without causing spreading (Figure S11)—-unlike Janus membranes (Figure S5).

2. Mechanism of unidirectional water transportation.

In this section, we first study the mechanics of water adhesion on the textile. The optimized patterned textile was applied to demonstrate an anti-gravity transfer of water in absence of beaded water droplet on its top side—without flooding the top surface of the patterned material, rather the transferred water rolls on the inclined patterned interface as shown in Figure 3A and Movie 3. The pattern interface is capable of rolling both directly beaded droplets on patterned top-spot and transferred water from patterned back-spot—with low difference in the volume of rolling droplets of water. The rolling of transferred water primarily depends on the water friction force. In this context, the water friction forces acting on the top side vary depending on the direction of the water supply, either from the top side or the bottom side of the textiles. In the case of supplying water from the top side, the water friction force is estimated following given equation in Eq.1.

$F_{c\,(Top)} = [\rho U t_c g - \pi d\gamma] \sin\alpha$ ……. Eq.1

where ρ: water density ≈ 997 kg m^{-3}, U: feed water flow rate, t_c: critical flow time for droplet sliding, g: gravitational acceleration constant ≈ 9.80065 m s^{-2}, d: syringe diameter ≈ 0.48 mm, γ: water surface tension ≈ 72.8 mN m^{-1}, α: textile tilting ≈ 45° (Figure 3B).
On the other hand, when the water was supplied from the bottom side (Figure 3C), friction force is estimated using Eq.2

$F_{c\,(Bottom)} = \rho U t_c g \sin\alpha$ …….. Eq.2

Figures 3D and 3E systematically studied the water friction forces, indicating that the force increased with the hydrophilic channel size $2r$ in variation of water-supplying sides and hydrophobic modifications on the background (Figures 3D and 3E).
Here, we hypothesized that the water friction force variation is owing to the pinning of the water contact line at the hydrophilic channel (Figure 3F).[36] In this model, the water friction is estimated by integrating the local pinning force ~$2r\gamma$ with the hydrophilic spot number near the contact line n, which yields $F_c \sim cn\gamma r$ where c is constant that should be influenced by the energy dissipation at the superhydrophobic area F_{SHPO}. Figure 3G shows the channel size dependence on $F_{c\,(Top)}$ to a log−log plot, in which the slope explains the power law of the r on $F_{c,}$ and the section value decreases with the increase of textile hydrophobicity.
Thereafter, we study the dynamics of water penetration through the textile (Figure 4A). When the feed water from the syringe contacts the superhydrophobic surface of the textile, the Laplace pressure P_{Lap} works to the water surface, depending on the curvature of the invading water surface. Here, the role of Laplace pressure is $P_{Lap} > 0$ for resisting or $P_{Lap} < 0$ for inducing water penetration. [37] In Figure 4B, the textile fiber diameter D ≈ 10 μm and inter-fiber interval W feature the textile geometry. The geometrical angle φ features the water invasion degree between the fibers. Θ is the water contact angle on the fiber. [38] From this model, the water surface curvature ε can be approximated to be $\varepsilon \approx 2\cos(\Theta-\Phi) / [W+D(1-\sin\Phi)]$ in the case of the $\Theta-\Phi > 0$. This estimation is applicable in the case of $\Theta-\Phi < 0$ by reversing the water−air phase. Thus, we obtain the Laplace pressure $P_{Lap} \approx \gamma\varepsilon \approx 2\gamma \cos(\Theta-\Phi) / [W+D(1-\sin\Phi)]$, where we estimated that the water curvature parallel to the fiber direction ≈ 0. While this, the water feed pressure is estimated to be $4F_{feed}/[\pi d^2]$, where F_{feed} is the hydrodynamic force in supplying water. Thus, the condition for the water penetration is $4F_{feed}/[\pi d^2] > P_{Lap}$ and *vice versa*.

In Figure 4C, we simulated the change in Laplace pressure when the textile wettability (Θ) and water invasion (Φ) were varied. This simulation explains how wettability variation and water invasion behavior change the mechanics of water penetration. For the simple estimation, we assumed $W \approx D$. We divided the water invasion state into four types depending on the plus/minus of P_{Lap} and $\varphi < 90°$ or $>90°$: (i) Laplace pressure works to resist water penetration in water penetrating more than half of the hydrophilic fiber; (ii) Laplace pressure works to induce water penetration in water penetrating more than half of the hydrophobic fiber; (iii) Laplace pressure works to resist water penetration with small water invasion between hydrophobic fibers, and (iv) Laplace pressure works to induce water penetration in the early stage of water invasion between hydrophilic fibers. In cases (i), (iii), and (iv), we use Θ as advancing contact angles. In case (ii), we use Θ as a receding contact angle.

When the water contacts the hydrophilic fiber ($\Phi = 180°$), the negative Laplace pressure induces wetting in a (iv) state, and water invasion proceeds (Φ gradually decreases). Then, Laplace pressure transitions from negative to positive with the decrease of Φ, and water penetration is resisted in a (i) state. Thus, hydrophilic textile induces the trapping of water between the fibers. In contrast, when the water contacts the hydrophobic fiber ($\Phi = 180°$), the positive Laplace pressure resists water penetration in a (iii) state despite the large Φ. However, when water invasion is proceeded by significant water feed pressure, Laplace pressure transitions to negative with the decrease of Φ, and water is detached from the fiber in a (ii) state. Thus, water does not remain inside the fibers of hydrophobic textiles. After that, to investigate the flow rate of unidirectional transport of water against gravity, the patterned textile was kept tilted at 45° (Figure 3A bottom panel) prior to feeding water to the back-spot of the patterned textile, maintaining a continuous flow rate of 10 μLs^{-1}. Within two seconds (Movie 3), the supplied water transferred to the top side of the PT_{60} and rapidly grew to a volume of 17 μL—and immediately rolled off from the top surface due to low water frictional force. Eventually, this experimental setup allowed us to measure the flow rate of the unidirectional transport of water against gravity—i.e. 8.5 μLs^{-1}. It is interesting to note that an elevation in the flow rate of transferred water was noticed on increasing hydrocarbon chain length of selected alkyl modifications (octyl, lauryl and octadecyl) as shown in Figure 4D. On the other hand, the patterning channel with a larger diameter affected the transfer of liquid—and its subsequent rolling on the top surface. This experiment indicates the need for precise control over channel dimension and chemical modulation to achieve a high flow rate for transporting water against gravity. It is worth to mention that the change in relative area between superhydrophobic to

hydrophilic regions on the top surface of the prepared pattern surface barely affects the anti-gravity flow rate of water as shown in Figure S12.

While a high flow rate is desired to attend immediate transport of water, an elevated breakthrough pressure prevents the backflow of accumulated across the patterned textile. Figure 4E estimates the macroscopic water penetration resistance of the textiles with channels. The hydrophilic channel size and water penetration direction (top or bottom sides) are changed here. Figure 4E shows the experimental setup, in which we feed water to pattern interface having differences in the diameter of channel size, and define the critical height for the feed water penetration H_c. We assume the critical pressure for the water penetration is concentrated in the channel area, which yields $H_c \sim r^{-2}$. Figure 4E shows the experimental results of the H_c with different r, where the slope of the plot validates the power raw between H_c and r. Moreover, we find that the water penetration resistance was largely influenced by the water penetration direction, where the background chemical modification has minimal influence. Thereafter, prepared pattern textile was utilized as a 'liquid diode', where readily penetration of water was noticed in a single direction of the patterned textile as shown in Figure 4F —i.e., from back-spot to top-spot—however, the flow of water in the reverse direction was completely restricted even at relatively high pressure created by water column of 6.7 cm in a commercially available intravenous transfusion tube as depicted in Figure 4G and Movie 4. Often, the venous pressure in the body leads to uncontrolled blood backflow into the infusion tube—which causes blood clots and other related unwanted medical complications. Such 'liquid-diode' would be useful in achieving a unidirectional and intravenous delivery of nutrition and medications—without causing backflow of blood during and after intravenous transfusion process. The inherently high breakthrough pressure on the top-spot of the patterned textile would be capable of avoiding the backflow of blood during such medical procedures. Moreover, this 'liquid-diode' would be further utilized in guided transport of liquid following an anti-gravitational pathway.

3. Durability and Performance of Patterned Coating

The prospective application of such patterned textiles in outdoor conditions is only possible if it remains tolerant to various abrasive physical and chemical exposures. In this context, widely accepted and standard physical abrasion tests were adopted to examine the stability of embedded superhydrophobicity of the coated textile.[39] Firstly, the superhydrophobic textile was subjected to tensile deformation with 125% repetitive strain for 1000 cycles—without compromising the embedded extreme water repellence (Figure S13A). Thereafter, an abrasive

sandpaper (400 grit (1 cm × 2 cm)) was rubbed with back-and-forth motion on the coated textile with an applied external pressure of 25 kPa, and water wettability was examined at regular intervals of abrasion distance. The coated textile remained superhydrophobic with WCA of ~ 150° even after incurring sandpaper abrasion with a distance of 5000 cm (Figure S13B). The prepared coating remained efficient in tolerating various and relevant physical manipulations—including bending, creasing, and twisting—without compromising the embedded superhydrophobicity (Figure S14A-F). Thereafter, to examine the chemical durability of the embedded superhydrophobicity, the coated textile was separately exposed to different chemically complex conditions—including seawater, river water, surfactant contaminated water, and UV irradiation for 6 weeks, prior to examining the water wettability (Figure S14G). The treated textile continued to display extreme water repellence—likely due to covalent modification of the reactive coating with selected hydrocarbons (i.e., octadecylamine and ODAc) through robust β aminoester type linkage. Next, the patterned textile was subjected to tensile deformation with 125 % strain—prior to sequentially exposing water droplets on top-spot and then on the back-spot. While the beaded water droplet on the top-spot failed to filtrate through the patterned textile under gravity—the blue coloured water droplet readily transported from the back-spot to the top-spot against the gravity with and without the applied strain of 125 % tensile deformation as depicted in Figure 5A-D. Moreover, the ability to unidirectionally transport beaded water on the patterned textile remained unaffected even after performing the adhesive tape peeling and sand drop tests. While in a standard adhesive tape peeling test, a freshly exposed adhesive tape was applied on the patterned textile with an external load of 1 kg and peeled off; 300 g of sand was dropped on the prepared material from a distance of 40 cm prior to demonstrating the unidirectional transport of water droplet as depicted in Figure 5E. The anti-gravity flow rate of the water across the patterned textile that was subjected to various physical abrasions or manipulations remained nearly unperturbed only except for patterned textiles that were exposed to adhesive tape peeling test or tensile deformations (Figure 5E). In such scenarios, the porosity and arrangement of fiber in the patterned textile are expected to be altered—which is likely to contribute to a slight depletion of flow rate of transferred water. The embedded superhydrophobicity of the fabric remained unperturbed even after incurring the standard washing test for 350 cycles (Figure S15). The above results are attributed to the durability of the patterned interface—which makes it more appropriate for its realistic application. Next, another important property, i.e., the breathability of textile, which helps to maintain health and hygiene of the skin was examined by studying the water vapor transmission rate (WVTR) as shown in Figure 5F. The WVTR of the patterned textile remained very similar

to the native fibrous substrates—as the deposition of reactive coating is less likely to affect the inherent pores of the fibrous substrate as revealed from the microscopic images (Figure S16). In general, a wet native textile is found to be sticky on wet skin. Hence, the force of adhesion of patterned textile was estimated and compared with respect to native textile under identical experimental conditions using a force tensiometer. In this context, both patterned and bare textiles were individually and similarly brought in contact with wet interface, and the force of adhesion was measured to detach bare and patterned textiles from the wet surface. The force of adhesion of the patterned textile is observed to be ~ 8 times less than that of the native textile as shown in Figure 5G. The depleted force of adhesion of the patterned textile certainly indicates the existence of non-sticky features at wet conditions—because of the unidirectional transport of water—which provided a dry interface. Thereafter, the water elimination performance by the patterned interface was demonstrated directly on the skin of a volunteer, prewetted with artificial sweat, prior to expose the back-side of the prepared pattern-textile. The Janus channel of the patterned textile ensured unidirectional transport of artificial sweat from the skin of a volunteer as depicted in the Figure 5H. Thus, the moist skin turned to be dry. On the contrary, bare textile failed to display such unidirectional and anti-gravity transport of artificial sweat, rather some traces of artificial sweat remained even after the similar exposure of bare textile to the pre-wetted (with artificial sweat) skin as demonstrated in Figure 5I. Thereafter, both bare and patterned textiles were placed on prewetted skin of a volunteer, prior to record the body surface temperature using an infrared camera. The difference in temperature was noticed to be 4.2°C. The ability of unidirectional transport of artificial sweat resulted in better cooling (31.5°C vs. 35.7°C) of patterned textile in comparison to bare textile, where the temperature of skin was recorded to be 36.9°C. This is likely due to faster evaporation of ejected artificial sweat by the patterned textile (Figure 5J), which is not possible to achieve with bare textile. However, such efficient cooling was not observed in absence of artificial sweat, and barely any difference in temperature was noticed between bare and patterned textile, (Figure 5K) and body temperature remained nearly similar, i.e. ~ 37.1°C. After that, we fabricated a large-scale pattern fabric with a dimension of A4 size printing paper (29.7 cm x 21 cm) in the laboratory without demanding any equipment, following the same principle of spatially selective chemical modification. In this context, a plastic mask with holes of specific dimensions (diameter of 1.5 mm) and arrangments (spacing of 1 cm) was placed on top of the chemically reactive superhydrophobic fabric before exposing it to glucamine solution, as depicted in Figure S13. The holes in the plastic mask allowed for spatially selective exposure of glucamine solution to chemically reactive superhydrophobic coating, enabling post-covalent

modification at ambient conditions. Consequently, we derived a well-ordered patterned fabric of a dimension of A4 size printing paper (29.7 cm x 21 cm), as shown in Figure 5L. Next, to demonstrate the versatility of the current coating and patterning approach, various other fibrous substrates—including lycra, polyester, cotton and wool were successfully coated following the same approach to attend superhydrophobic state—maintaining residual chemical reactivity (Figure S18). Further, spatially selective chemical modification provided patterns on such reactive superhydrophobic coating deposited on various fibrous substrates to depict anti-gravity transfer of water as shown in Figure 5M-P. Thus, our current approach of direct chemical modulation provided a general basis to develop Janus patterned coating, irrespective of the nature of the selected textile. Finally, the cell viability study was performed on pattern fabric—and the result was compared with respect to the bare, glucamine modified fabric and tissue culture plate (TCP). The selected textiles of dimension 4.5 cm x 4.5 cm were incubated in a cell culture medium for 24 hours prior to perform MTT assessment on human dermal fibroblast (HDF) cells. The study revealed a minimal change in the cellular viability between the various fabric leachate mediums (LM) and positive control (i.e. TCP) after 48 h (Figure S19). Moreover, morphologies of the seeded HDFs were observed using the phalloidin-hoechst 33342 staining after 48 h of treatment with LM from various fabric groups and compared with the untreated control and representative micrographs have been shown in Figure S20A-D. The cellular morphologies of HDFs treated with LM from bare fabric (Figure S20B), patterned fabric (Figure S20C) and glucamine treated fabric (Figure S20D) demonstrated minimal deviations from the cellular morphology observed for untreated HDFs (Figure S20A). Thus, the prepared pattern textiles remained compatible for potential interaction with and/or exposure to skin tissue. Further, the ability of prepared patterned textile in fast removal of aqeouse phase against the gravity is likely to be useful in relavent bio-medical applications—including wound healing, where the prepared patterned textile would help in keeping the wound dry and clean by removing the excess biofluid from the site of the wound.

Conclusions:

In summary, the current approach of preparing a chemically reactive superhydrophobic coating on fibrous substrate provided a facile basis to develop Janus patterns of chemically-modulated wettability with extremely water-repellent background through spatially selective 1,4-conjugate addition reaction with hydrophilic small molecules—i.e. glucamine. The prepared Janus patterned remained efficient for anti-gravity transporting the water droplets—with a record high flow rate with respect to the relevant reported literature. The fast flow of liquid attributes to the

favourable pinning and depinning mechanism of invaded water through such chemically decorated patterns on selected fibrous substrates. Further, rational choice of other hydrophilic small molecules is likely to provide a scope to improve the process versatility and functionality of such pattern interfaces. In contrast to reported Janus textile, the design of Janus patterns on superhydrophobic background prevents the flooding of the top surface of the patterned textile, rather transported water rolled off easily on the tilted interface because of the embedded low frictional force. The prepared Janus pattern of wettability with the ability of unidirectional anti-gravity transfer of tiny and relevant aqueous droplets across the fibrous substrates demonstrated efficient ejection of artificial sweat and management of temperature. Further, the fast and unidirectional anti-gravity flow of liquid with high breakthrough pressure would be useful in achieving accelerated wound healing, developing liquid diode etc. Importantly, the prepared Janus pattern remained efficient to tolerate exposure of various and severe physical (i.e., physical manipulations, tensile deformation, adhesive tape peeling, sandpaper abrasion) and chemical exposures (e.g., seawater, river water, UV light, repetitive washing etc.). Furthermore, the current approach of depositing reactive superhydrophobic coating and followed by spatially selective chemical patterning through 1,4-conjugate addition reaction with primary amine containing small molecules at ambient condition can be successfully applied on various types of textiles. The current design is not restricted to a specific type of textile, hence, it would be more appropriate for multiple prospective applications in diverse and realistic conditions.

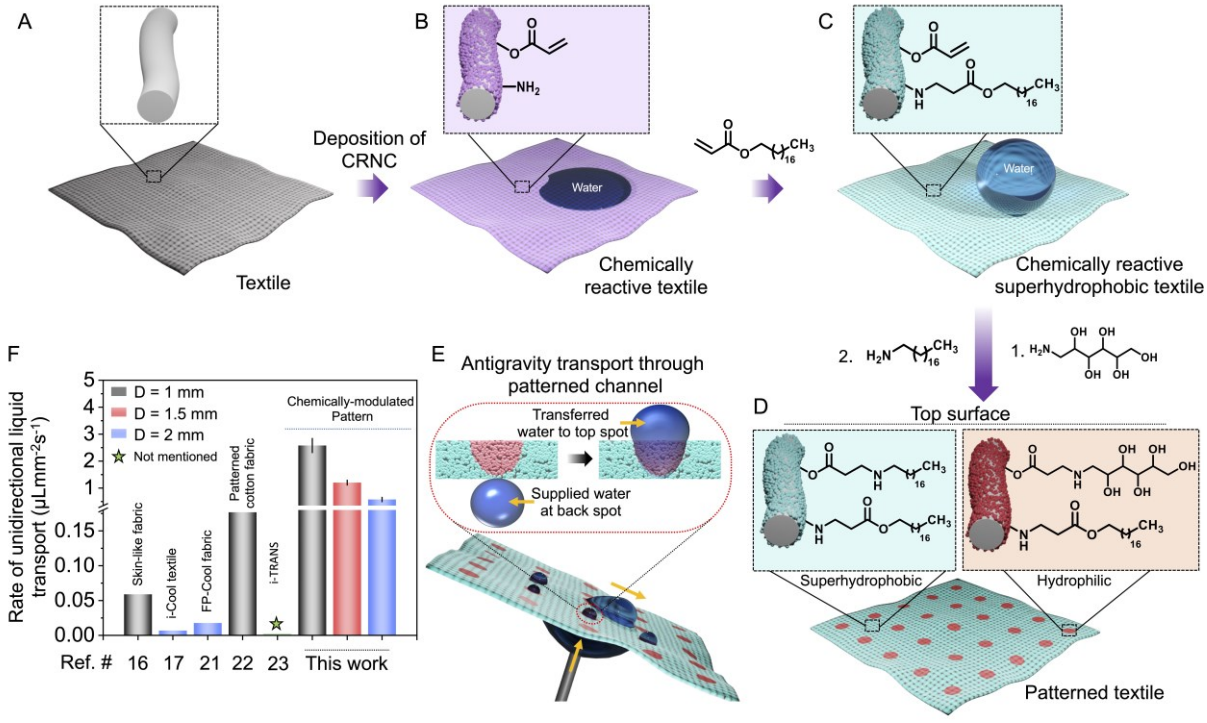

Scheme 1. (A-D) In situ, deposition of chemically reactive nano complex (CRNC) derived from a reaction mixture of 5Acl and BPEI on a selected textile (A) following the dip coating process

yielded chemically reactive textile (B). Its post-chemical modifications with octadecyl acrylate (ODAc) conferred superhydrophobicity—and denoted as a chemically reactive superhydrophobic textile(C). The spatially selective modification of chemically reactive superhydrophobic textile with glucamine followed by octadecylamine provided Janus channels on a chemically inert superhydrophobic background. E) Schematic illustrating the unidirectional transport of beaded droplets through patterned textiles against gravity. F) The plot compares the rate of unidirectional transport against the gravity of current work with the reported literature [ref # 16, 17, 21, 22, 23]. Results are presented as mean ± SD, where sample size, n = 3.

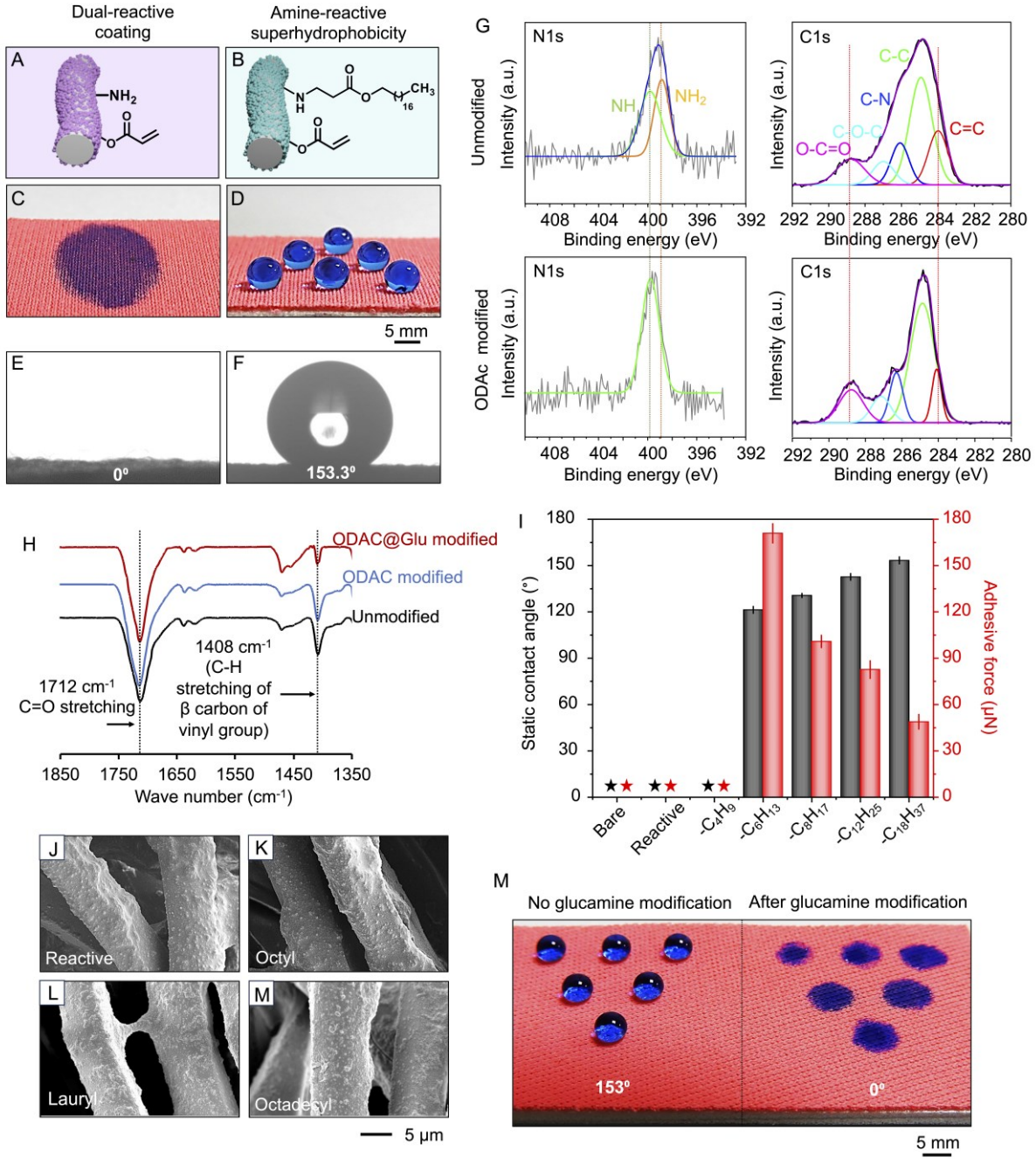

Figure 1. (A-F) Schematic representations (A and B), digital images (C and D), and contact angle images (E and F) of a dual reactive coating before and after ODAc modification. G) High-

resolution XPS spectra with deconvolution for N 1s (left panel) and C 1s (right panel) before and after chemical modifications of dual reactive coating with ODAc. H) FTIR spectra of dual reactive coating before and after modification with ODAc, followed by glucamine. I) Plot illustrating the static water contact angle and adhesion force of dual reactive coating after modifying with different alkyl acrylate. Star sign indicated instant soaking of beaded water droplet by the respective textiles. (J-M) FESEM images of dual chemically reactive coated textile before (J) and after octyl (K), lauryl (L), and ODAc (M) modifications. (N) Digital image and contact angle images of a chemically reactive superhydrophobic interface after modifying half (right-side) of it with glucamine. Results are presented as mean ± SD, where sample size, n = 3.

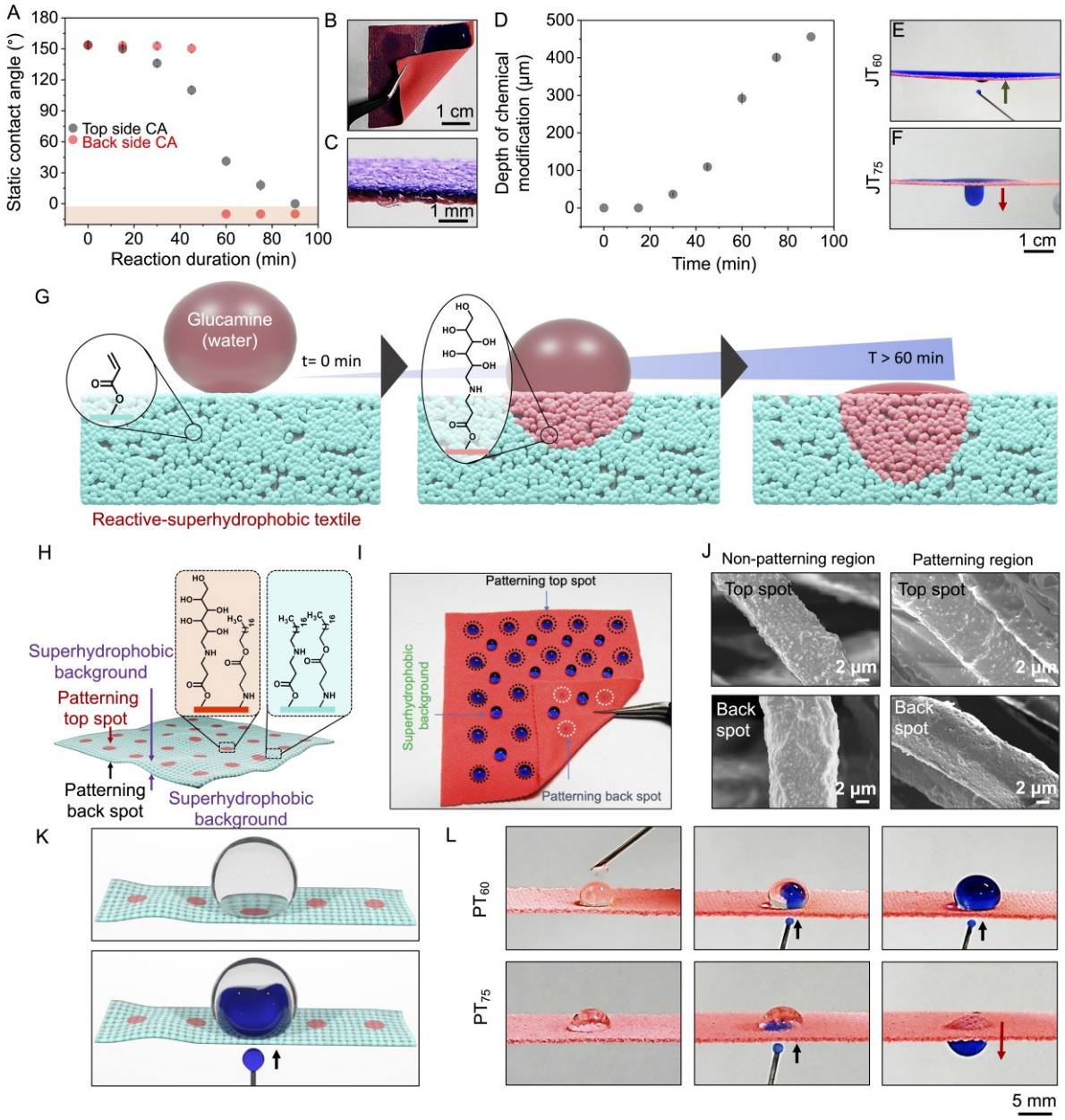

Figure 2. A) The plot illustrating static WCAs of beaded water on the top and back-sides of the chemically reactive superhydrophobic textile after glucamine treatment for different durations. B) Digital images of modified textile with Janus wettability, where beaded water (blue colored)

droplets spread on the top surface, and the bottom surface remained dry. C) Digital image of a cross-sectional view of the same textile. D) This plot illustrates the depth of chemical modification of textiles with the progress of reaction time with glucamine. (E-F) Digital images depicting anti-gravity transport of blue-colored water droplets across the Janus textiles derived through modifying reactive superhydrophobic textile with glucamine for different durations—i.e., 60 min (E) and 75 min (F). (G) This schematic illustrates the spatially selective glucamine modifications on reactive-superhydrophobic textile—through gradual infiltration of beaded aqueous droplets of glucamine. Current approach provides easy control over patterning size and depth. H) Schematic of a chemically patterned superhydrophobic interface, where hydrophilic spots, denoted by red colors, were achieved on a superhydrophobic background via spatially selective chemical modifications. I) Digital images depicting the difference in wetting of beaded water droplets on pattering top-spots (indicated with dotted black circle), and pattering back-spots (depicted with dotted white circle). While the beaded water displayed a low contact angle on patterning top-spot—the droplet readily soaked on placing into the pattering back-spot. The background on both surfaces repelled the beaded water extremely, causing it to appear spherical. J) FESEM images on patterning and non-patterning regions at the top and back sides of the patterned textile. (K-L) This schematic depicts the unidirectional transport of blue-colored water against gravity to the beaded droplet on the top of the patterned textile. L) Digital images account for the ability of two distinct patterned textiles (PT_{60} and PT_{75}) towards anti-gravity water transportation. Results are presented as mean ± SD, where sample size, n = 3.

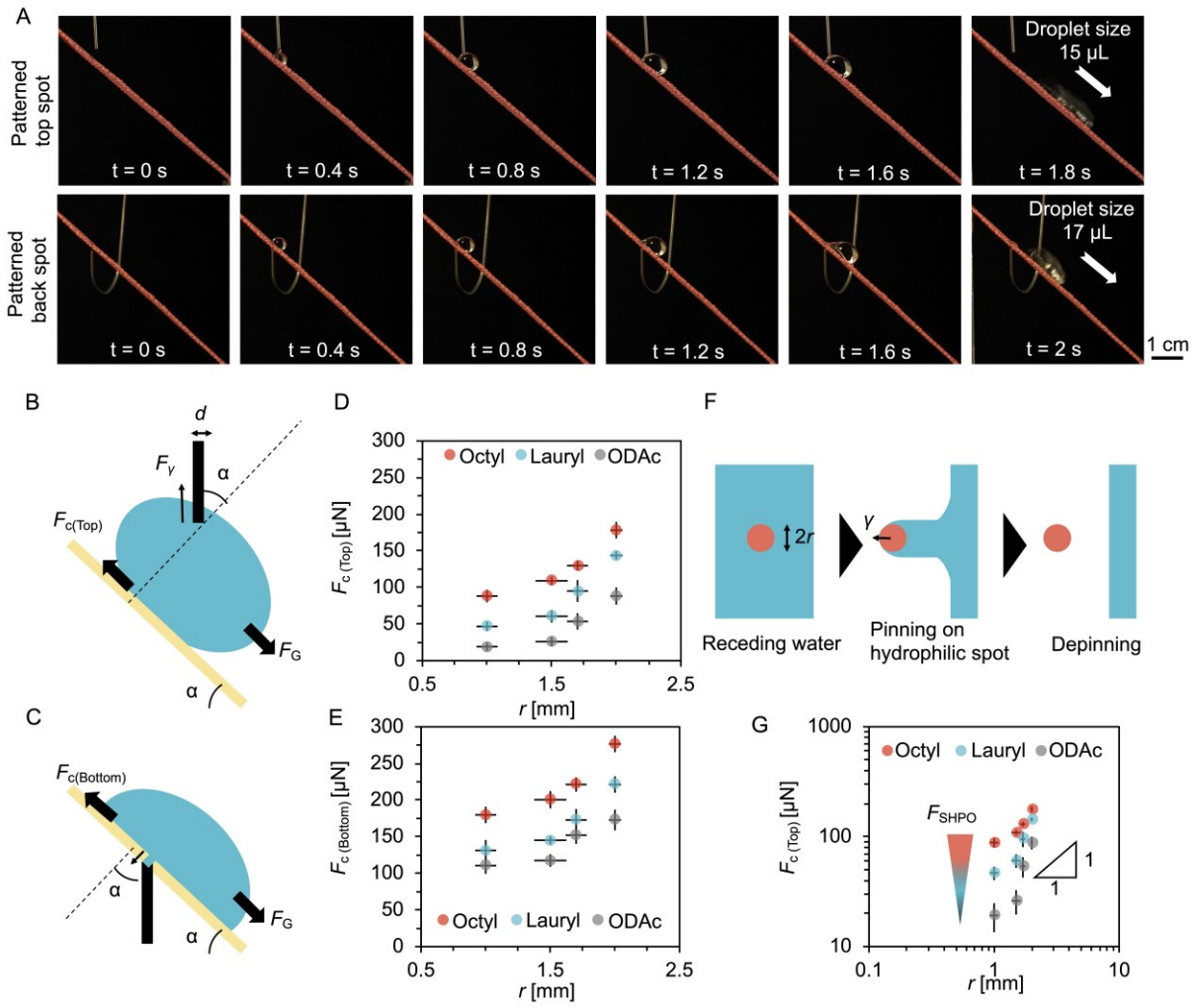

Figure 3. A) Digital images accounting for the rolling of beaded (from the top side) and transported water droplets (from the back side) on patterned textile that was kept inclined at an angle of 45°. (B, C) Side view schemes of adhesion mechanics of water fed from (B) top-side or (C) bottom-side of the textile. (D, E) Water friction force as a function of channel size. (D)Water is fed from the top side or (E) the bottom side. (F) Top-view scheme of the contact-line-depinning behavior of the water on the superhydrophobic textile with hydrophilic spot. (G) Log-log plot of water adhesion force as a function of channel size in case of water supplied from the top side. Results are presented as mean ± SD, where sample size, n = 3.

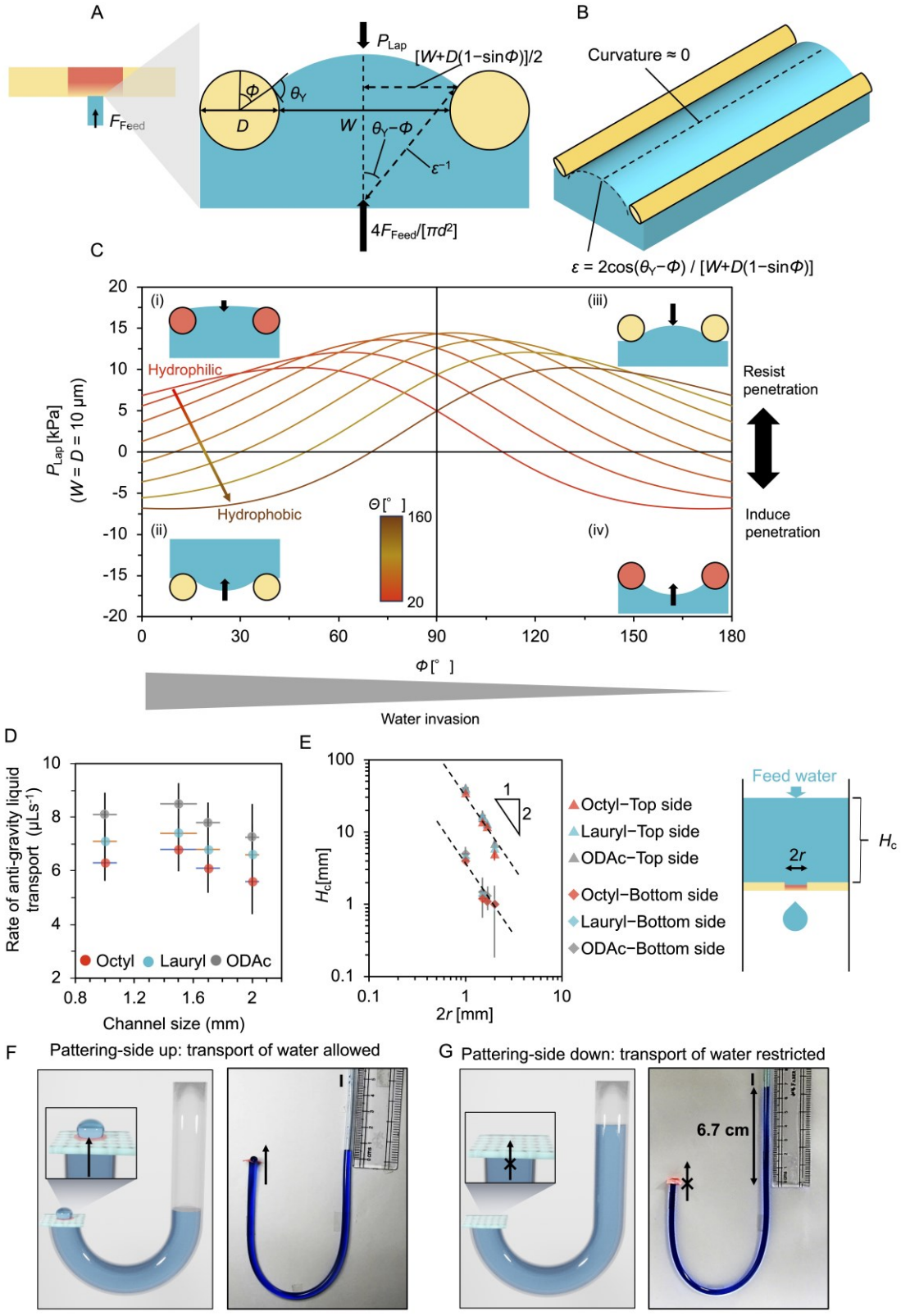

Figure 4. A-B) Scheme of feed water penetrating behavior between superhydrophobic textiles. The textile fiber diameter D and inter-fiber interval W feature the textile geometry. The geometrical angle φ features the water invasion degree between the fibers. Θ is the water contact angle on the fiber. C) Estimating the Laplace pressure PLap with different fiber wettability (that is Θ ranging from 20 to 160°) and water invasion φ in case of W = D = 10 μm. D) Plot illustrating the change in water flow rate with a variation of channel dimensions and chemical modification in the background. E) The plot accounting for the change in water penetration

resistance on the variation of the dimension of channels and chemical modifications at the background of the channel, and the scheme displays the experimental setup. F-G) Depicting the patterned textile as a 'liquid diode', where one end of the intravenous transfusion tube was covered with patterned textile—keeping the pattering spot inverted. The penetration of water was noticed from the back side when the water level on the other side of the tube was slightly elevated (F); however, such transportation of water was not observed even though the difference in the water columns in left and right side of the tube was kept at 6.7 cm as the pattern textile was kept inverted to exposed the patterning side towards the interior of the tube (G). Results are presented as mean ± SD, where sample size, n = 3.

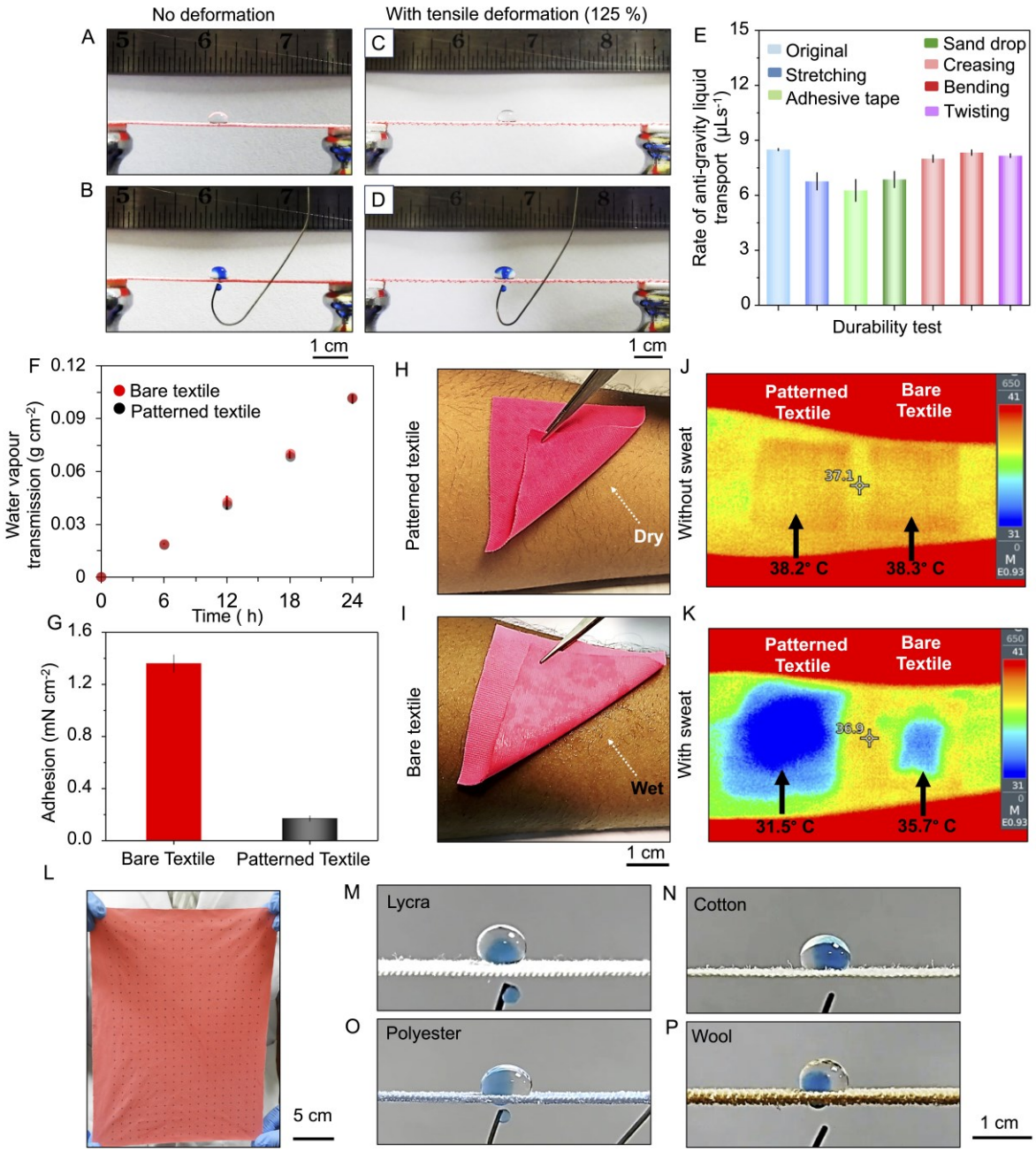

Figure 5. (A-D) Digital images illustrating the unidirectional and anti-gravity transport of water through the patterned textile in the absence (A, B) and presence (C, D) of 125 % tensile deformation. E) Plot accounting for the rate of anti-gravity transport of water through patterned textiles after performing different types of physical abrasion tests. F) Accounting water vapor transmission rates through the bare and patterned textiles. G) Adhesion forces of bare and patterned textiles on wet surfaces. (H-I) digital images depict artificial sweat transport by patterned (H) and bare (I) textiles. (J-K) Infrared camera images of the patterned and bare textiles applied on the skin in artificial sweat's absence (J) and presence (K) were recorded outdoors at a surrounding temperature of 40°C. (L) The spatially selective chemical modification allowed scalable fabrication of patterned textiles at ambient conditions without using any equipment. (M-P) Illustrating the unidirectional water transport ability of the patterned interfaces developed on various fibrous substrates—including lycra, (M) cotton, (N) polyester, (O) and wool (P). Results are presented as mean ± SD, where sample size, n = 3.

Acknowledgments

Science and Engineering Research Board (CRG/2022/000710) and Ministry of Electronics and Information Technology (no. 5(1)/2022-NANO) are acknowledged for financial support. U.M. thanks CIF, CFN, SHST and the Department of Chemistry, Indian Institute of Technology Guwahati, for their generous assistance in executing various experiments and for the infrastructures. S.K. thanks the institute and Ministry of Education for PhD fellowship.

References:

[1] J. Ju, H. Bai, Y. Zheng, T. Zhao, R. Fang, L. Jiang, *Nat. Commun.* **2012**, *3*, 1247.
[2] S. Zhang, M. Chi, J. Mo, T. Liu, Y. Liu, Q. Fu, J. Wang, B. Luo, Y. Qin, S. Wang, S. Nie, *Nat Commun.* **2022**, *13*, 4168.
[3] Y. Zheng, H. Bai, Z. Huang, X. Tian, Fu-Q. Nie, Y. Zhao, J. Zhai, L. Jiang, *Nature* **2010**, *463*, 640–643.
[4] J. Chen, A. Tsuchida, A. D. Malay, K. Tsuchiya, H. Masunaga, Y. Tsuji, M. Kuzumoto, K. Urayama, H. Shintaku, K. Numata, *Nat. Commun.* **2024**, *15*, 527.
[5] M. Prakash, D. Quere, J. W. M. Bush, *Science* **2008**, *320*, 931-934.
[6] S. Martin, B. Bhushan*, Phil. Trans. R. Soc. A.* **2016***, 374*, 20160134.
[7] TS. Wong, S. H. Kang, S. K. Y. Tang, E. J. Smythe, B. D. Hatton, A. Grinthal, J. Aizenberg, *Nature* **2011**, 477, 443–447.
[8] S. Anand, A. T. Paxson, R. Dhiman, J. D. Smith, K. K. Varanasi, *ACS Nano* **2012**, *6*, 10122–10129.
[9] H. Chen, P. Zhang, L. Zhang, H. liu, Y. Jiang, D. Zhang, Z. Han, L. Jiang, *Nature* **2016**, *532*, 85–89.
[10] X. Dai, N. Sun, S. O. Nielsen, B. B. Stogin, J. Wang, S. Yang, TS. Wong, *Sci. Adv.* **2018**, *4*, eaaq0919.
[11] H. Bai, X. Wang, Z. Li, H. Wen, Y. Yang, M. Li, M. Cao, *Adv. Mater*. **2023**, *35*, 2211596.
[12] Z. Liu, Z. Zhan, T. Shen, N. Li, C. Zhang, C. Yu, C. Li, Y. Si, L. Jiang, Z. Dong, *Nat. Commun.* **2023,** *14*, 4128.
[13] C. Yang, M. Long, C. Ding, R. Zhang, S. Zhang, J. Yuan, K. Zhi, Z. Yin, Y. Zheng, Y. Liu, H. Wu, Z. Jiang, *Nat. Commun*. **2022,** *13*, 7334.
[14] D. Wakerley, S. Lamaison, F. Ozanam, N. Menguy, D. Mercier, P. Marcus, M. Fontecave, V. Mougel, *Nat. Mater*. **2022,** *13*, 7334.
[15] T.-H. Shen, L. Spillane, J. Peng, *Nat. Catal* **2022,** *5*, 30-36.
[16] L. Lao, D. Shou, Y. S. Wu, J. T. Fan, *Sci. Adv*. **2020**, *6*, eaaz0013.
[17] Y. Peng, W. Li, B. Liu, W. jin, J. Schaadt, J. Tang, G. Zhou, G. Wang, J. Zhou, C. Zhang, Y. Zhu, W. Huang, T. Wu, K. E. Goodson, C. Dames, R. Prasher, S. Fan, Y. Cui, *Nat. Commun.* **2021,** *12*, 6122.
[18] A. Ainla, M. M. Hamedi, F. Güder, G. M. Whitesides, *Adv. Mater*. **2017**, *29*, 1702894.
[19] Z. Zhao, Y. Ning, S. Ben, X. Zhang, Q. Li, C. Yu, X. Jin, K. Liu, L. Jiang, *Adv. Sci*. **2022**, *9*, 2103765.
[20] B. Dai, K. Li, L. Shi, X. Wan, X. Liu, F. Zhang, L. Jiang, S. Wang, *Adv. Mater*. **2019**, *31*, 1904113.
[21] F. Li, S. Wang, Z. Wang, K. Jiang, X. Zhao, L. Shao, Y. Pan, *Adv. Funct. Mater.* **2023**, *33*, 2210769.

[22] Y. Lin, N. Cheng, N. Meng, C. Wang, X. Wang, J. Yu, B. Ding, *Adv. Funct. Mater.* **2023**, *33*, 2304109.
[23] Y. Peng, J. Zhou, Y. Yang, J.-C. Lai, Y. Ye, Yi Cui, *Adv. Mater*. **2022**, *34*, 2204168.
[24] W. Zhou, S. Min, T. Zhan, Y. Zhang, D. Pan, Y. Yuan, B. Xu, *Small* **2023**, 2302512.
[25] W. Shi, H. Bai, M. Cao, X. Wang, Y. Ning, Z. Li, K. Liu, L. Jiang, *Adv. Sci.* **2023**, *10*, 2301421.
[26] Y. Wang, X. Liang, H. Zhu, J. H. Xin, Q. Zhang, S. Zhu, *Adv. Funct. Mater.* **2020**, *30*, 1907851.
[27] Y. Wang, G. Xia, H. Yu, B. Qian, Y. H. Cheung, L. H. Wong, J. H. Xin, *Adv. Mater.* **2021**, *33*, 2100140.
[28] B. Gu, Q. Xu, H. Wang, H. Pan, D. Zhao, *ACS Nano* **2023**, *17*, 18308–18317.
[29] W. Fan, G. Zhang, X. Zhang, K. Dong, X. Liang, W. Chen, L. Yu, Y. Zhang, *Small* **2022**, *18*, 2107150.
[30] H. Murota, K. Yamaga, E. Ono , N. Murayama, H. Yokozeki , I. Katayama *Exp Dermatol*. **2019**, *28* 1416–1421.
[31] J. Fan, Y. S. Chen, *Meas. Sci. Technol.* **2002**, *13*, 1115–1123.
[32] D. J. Gohlke, J. C. Tanner, *J. Coated Fabrics* **1976**, *6*, 28–38.
[33] A. Mukhopadhyay, V. K. Midha, *J. Ind. Text.* **2008**, *38*, 17–41.
[34] A. Borbora, R. L. Dupont, Y. Xu, X. Wang, U. Manna, *Mater. Horiz.* **2022**, *9*, 991–1001.
[35] M. Dhar, U. I. Kara, S. Das, Y. Xu, S. Mandal, R. L. Dupont, E. C. Boerner, B. Y. Chen, Y. X. Yao, X. G. Wang, U. Manna, *Mater. Horiz.* **2023**, *10*, 2204 –2214.
[36] P.-G. de Gennes, F. Brochard-Wyart, D. Quéré, in *Capillarity and Wetting Phenomena: Drops, Bubbles, Pearls, Waves* (Eds: P.-G. Gennes, F. Brochard-Wyart, D. Quéré), Springer, New York 2004, p. 153.
[37] G. Zhang, M. A. Quetzeri-Santiago, C. A. Stone, L. Botto, J. R. Castrejón-Pita, *Soft Matter* **2018**, *14*, 8182-8190.
[38] A. Tuteja, W. Choi, J. M. Mabry, G. H. McKinley, R. E. Cohen, *Proc. Natl. Acad. Sci. USA* **2008**, *105*, 18200.
[39] X. Tian, T. Verho, R. H. A. Ras, *Science*, **2016**, *352*, 142-143.

Supplementary information

The online version contains supplementary material.

Conflict of Interest

The authors declare no conflict of interest

Data Availability Statement

The data presented in this article are available from the corresponding authors on reasonable requests.

Table of Contents Entry:

A water-based facile 1,4-conjugate addition reaction at ambient conditions is introduced to orthogonally modulate chemically reactive coated textile for developing spatially selective

channels with Janas wettability on a water-repellent background. The current method of chemically modulated patterning allows precise control of channel dimension and wettability contrast to achieve a superior flow rate (8.5 μLs^{-1}) of anti-gravity water transportation. The patterning method was successfully applied to various types of textiles. Moreover, the prepared patterned interface remained tolerant to multiple and severe physical and chemical abrasions.

Keywords: Patterned textile • Moisture managment • superhydrophobicity • Anti-gravity transport • 1,4-conjugate addition reaction

Controlled Chemical-Patterning of Textile to Accelerate Anti-gravity Water Flow

*Saurav Kumar,[a] Angana Borbora,[a] Pritha Chakraborty,[a] Hrisikesh Sarma,[a] Ashutosh Bandyopadhyay,[d] Akash Bose,[a] Biman B. Mandal,[b,c,d] Mizuki Tenjimbayashi, [*e] Uttam Manna[*a,b,c]*